DOI: 10.21062/mft.2024.009 http://www.journalmt.com

Dilatometric Effects Accompanying Phase Transformations during Tempering of Spring Steels

Jakub Kotous (0000-0001-9141-8477), Zbyšek Nový (0000-0001-6976-1578), Petr Motyčka (0000-0002-2493-0494), Pavel Salvetr (0000-0001-5717-267X)
COMTES FHT a. s., Prumyslova 995, 334 41 Dobrany. Czech Republic.
E-mail: jkotous@comtesfht.cz, znovy@comtesfht.cz, pmotycka@comtesfht.cz, psalvetr@comtesfht.cz.

The tempering procedure of quenched 54SiCr6 spring steel was analyzed using continuous heating dilatometry, isothermal dilatometry, metallography, and hardness measurement. The dilatometry was performed on four different steel modifications with graduated Si content and with two levels of Cu. Metallography and hardness measurement were analyzed only on samples with one Si level. Two types of tempering procedures were compared in this experimental program. The first one was simple one-step tempering, the other was a special procedure of strain assisted tempering (SAT), which includes double tempering and strain applications between tempering. A dilatometry analysis with the support of metallography contributes to the material behaviour explanation, which is considerably different in both processing cases.

Keywords: Dilatometry, Strain assisted tempering, Nano-twins, Spring steel

1 Introduction

The tempering of hardened steels is a technological step, that brings the final adjustment of bulk material properties. It eliminates internal stress after quenching but also controls the final combination of properties like yield and ultimate strength, elongation, toughness, and others. During the tempering of spring steels, i.e. low alloy steels with middle carbon content, powerfull transformation effects take place. The precipitation of transition carbides, precipitation of cementite and other carbides respectively, and retained austenite decomposition are the most common and most important phenomena taking place during tempering. They are described in numerous literary sources [1-4].

Dilatometry is a type of thermo-physical analysis, that can be advantageously used to detect temperature ranges of transformations and other occurring effects during tempering [5-8]. The processes related to the precipitation of any type of carbides exhibit a shortening of the sample during an isothermal tempering process or a negative deviation from the linear growth during continual heating in the dilatometer [9]. On the contrary, the carbides dissolution similar like austenite decomposition is accompanied by volume increase. Dilatometer samples elongation or a positive deviation from linear growth during continual heating are observed [6,7]. In this way, aAl in ste dilatometry analysis seems to be a very useful tool for research, development, or optimization of the technological processing of hardened steels, in the current study, particularly concerning spring steels.

Transport means producers are currently facing many challenges due to escalating customer expectations and emerging standards. Decreasing the mass of components and increasing their reliability at the same time is among the most significant trends regarding mechanical and materials engineering aspects. There are two basic ways to approach the issue when trying to lose weight. The first way is using materials with lower density [10,11], the other way is using powerful materials with the potential to redesign components and reduce their robustness. The improvement of mechanical properties combination is the current topic for research and development of springs and materials for their production as well [12]. The optimization of both chemical composition and technological process chain aims at improving different parameters nevertheless the combination of strength, fatigue, reduction of area, and toughness seems to be the most frequently asked properties to be enhanced [13-16]. Barani and coll. [17, 18] have published several papers besides documenting the influence of high temperature and thermomechanical processing on mechanical properties.

Authors [19] describe a different way to achieve a better combination of fatigue and strength parameters during hardening. The strain assisted processing (SAT) consisting of the double tempering steps after quenching and carrying out the controlled strain between both tempering operations was developed to achieve a unique combination of transformation,

deformation, and precipitation strengthening in the hardened martensitic structure. Middle carbon low alloyed steel reveals very high yield strength and tensile strength and at the same time very attractive fatigue properties and toughness [19, 20]. This influence of SAT process on mechanical properties is currently not accompanied by a detailed explanation. The questions like which physical effects during this processing are going on, which type of strengthening is dominant, and which mechanism of deformation is active during the strain application remain unanswered. The current study uses mainly dilatometry analysis supported by metallography analysis and hardness measurement for a better understanding of phenomena during SAT process execution.

2 Materials and methods

The material under investigation was modified medium carbon steel based on conventional spring steel 54SiCr6 that is often used in stressed spring and flexible elements for cars and rolling stock. The cast BX corresponds to standard according to ČSN EN 10 089. The others casts (A, B, D) are modified by copper with differed content of silicon. Copper causes precipitation strengthening at tempering over 400 °C. And variable silicon content was choosen as suitable tool for regulation of strength-fragility. The chemical composition determined using a Q4 TASMAN optical emission spectrometer (Bruker Elemental GmbH, Kalkar, Germany) is given in Tab. 1.

Tab. 1 *The steels' chemical compositions and standard 54SiCr6 steel composition according to ČSN EN 10 089, wt.%*

Steel	C	Si	Mn	Cr	P	S	Cu	Fe
54SiCr6	0.51-0.59	1.20-1.60	0.50-0.80	0.50-0.80	<0.025	<0.025	<0.60*	bal.
BX	0.57	1.51	0.68	0.75	0.008	0.003	0.12	bal.
A	0.55	1.06	0.67	0.77	0.010	0.003	1.47	bal.
B	0.56	1.54	0.70	0.77	0.011	0.003	1.48	bal.
D	0.57	2.49	0.75	0.77	0.011	0.004	1.47	bal.

*Criterion <0.60 applies for Cu+10Sn. Content of tin in all steel was <0.007 wt.%

The ingots of all smeltings were brought to 1050 °C, hot rolled to a 14 mm thick sheet and air cooled. Normalization annealing was carried out at 850 °C for 40 min. Cylindrical samples, 13 mm in diameter and 120 mm in length were manufactured. The subsequent processing of all samples is presented in Tab. 2 and Tab. 3.

Tab. 2 *The processing of samples with final anisothermal heating in the dilatometer*

Sample designation	Processing of samples before the dilatometry analysis			Continual heating in the dilatometer
	Quenching temperature	The 1st tempering	Strain	
BX -C	900 °C	-	-	3 °C/min up to 700 °C
BX 250-C		250 °C/2 hours	-	
BX s250-C			17 %	
BX 350-C		350 °C/2 hours	-	
BX s350-C			17 %	
A -C	900 °C	-	-	3 °C/min up to 700 °C
A 250-C		250 °C/2 hours	-	
A s250-C			17 %	
A 350-C		350 °C/2 hours	-	
A s350-C			17 %	
B -C	900 °C	-	-	3 °C/min up to 700 °C
B 250-C		250 °C/2 hours	-	
B s250-C			17 %	
B 350-C		350 °C/2 hours	-	
B s350-C			17 %	
D -C	900 °C	-	-	3 °C/min up to 700 °C
D 250-C		250 °C/2 hours	-	
D s250-C			17 %	
D 350-C		350 °C/2 hours	-	
D s350-C			17 %	

Tab. 3 *The processing of samples with final isothermal heating in the dilatometer*

Sample designation	Processing of samples before the dilatometry analysis			Isothermal heating in the dilatometer
	Quenching temperature	The 1st tempering	Strain	
BX -350	900 °C	-	-	350 °C/2 hours
BX -400				400 °C/2 hours
BX s250-350		250 °C/2 hours	17 %	350 °C/2 hours
BX s250-400				400 °C/2 hours
B -350	900 °C	-	-	350 °C/2 hours
B -400				400 °C/2 hours
B s250-350		250 °C/2 hours	17 %	350 °C/2 hours
B s250-400				400 °C/2 hours

The quenching temperature was 900 °C with a twenty-minutes holding time. Quenching medium was oil. The following tempering was performed in an electric furnace or alternatively in the dilatometer. The cooling was in still air. The strain of 17 % was realized using the rotary swaging machine.

The anisothermal and isothermal dilatometry, metallography, and hardness measurement were done to describe the material's behavior during tempering after different preliminary processing. Dilatometry was performed on the L75PT dilatometer (Linseis, Selb, Germany) with samples heated in a furnace for heating at lower heating rates. Further, the quenching dilatometer L78 RITA (Linseis) was used for quenching and heating at 0.1 °C/s and higher rates. The experiments were performed in pure nitrogen, and the specimens were held in quartz glass push rods with a contact force of 0.3 N.

The metallographic samples were prepared by mechanical grinding and polishing in the longitudinal direction of specimens. The microstructure was revealed by etching in 3% Nital, and it was observed using light microscopy (NIKON ECLIPSE MA200; NIKON, Tokyo, Japan), scanning electron microscopy - SEM (JEOL IT 500 HR; JEOL, Tokyo, Japan) and transmission electron microscopy (JEOL 050422, PIPSTALOS 160522).

3 Results and discussion

3.1 Dilatometry analysis of tempering processes

The results of the continuous heating experiment are shown in Fig. 1, showing relative elongation from zero-elongation baseline measured during the continuous heating up to 700 °C. The zero-baseline is supposed to represent thermal elongation without transformations.

Full black curves (a) represent the continual heating of the quenched sample. Blue and green curves (b,c) show the heating after quenching and the first isothermal tempering at 250 °C. Yellow and red curves (d,e) represent the heating after the first isothermal tempering at 250 °C and following 17 % strain.

It is possible to follow different transformation phenomena through recorded dilatometry courses. The full black curves (a) could be considered a basic course where standard tempering phenomena just after quenching can be followed. The first deviation from the linear course can be observed in the temperature range between 100 and 200 °C. This deviation is negative, the sample becomes shorter compared to the ideal linear behavior. The shortening could be explained by transition carbides precipitation, which is visible in all examined materials. Applying the continuing heating this deviation is eliminated by BX and A material modification, the temporary growth of black curves by those materials in the temperature range from 250 to 350 °C may be related to the starting decomposition of retained austenite. Materials B and D do not reveal such a temporary growth.

All materials record considerable decreases in the temperature range close to 400 °C, where cementite precipitation is dominant and overcharges other reactions, e.g. austenite decomposition. From 400 °C all examined materials show only the negative deviation of black curves (a) and this deviation continually increases up to 700 °C.

A comparable course shows the samples which undergo continuous heating after quenching and the first isothermal heating at 250 °C (b-blue and c-green curves). The only significant difference from the samples without the first isothermal heating is the absence of the decrease due to transition carbides precipitation. In those cases, the transition carbides were already precipitated during the first isothermal heating. The next course of b-blue and c-green curves is very similar to the black record.

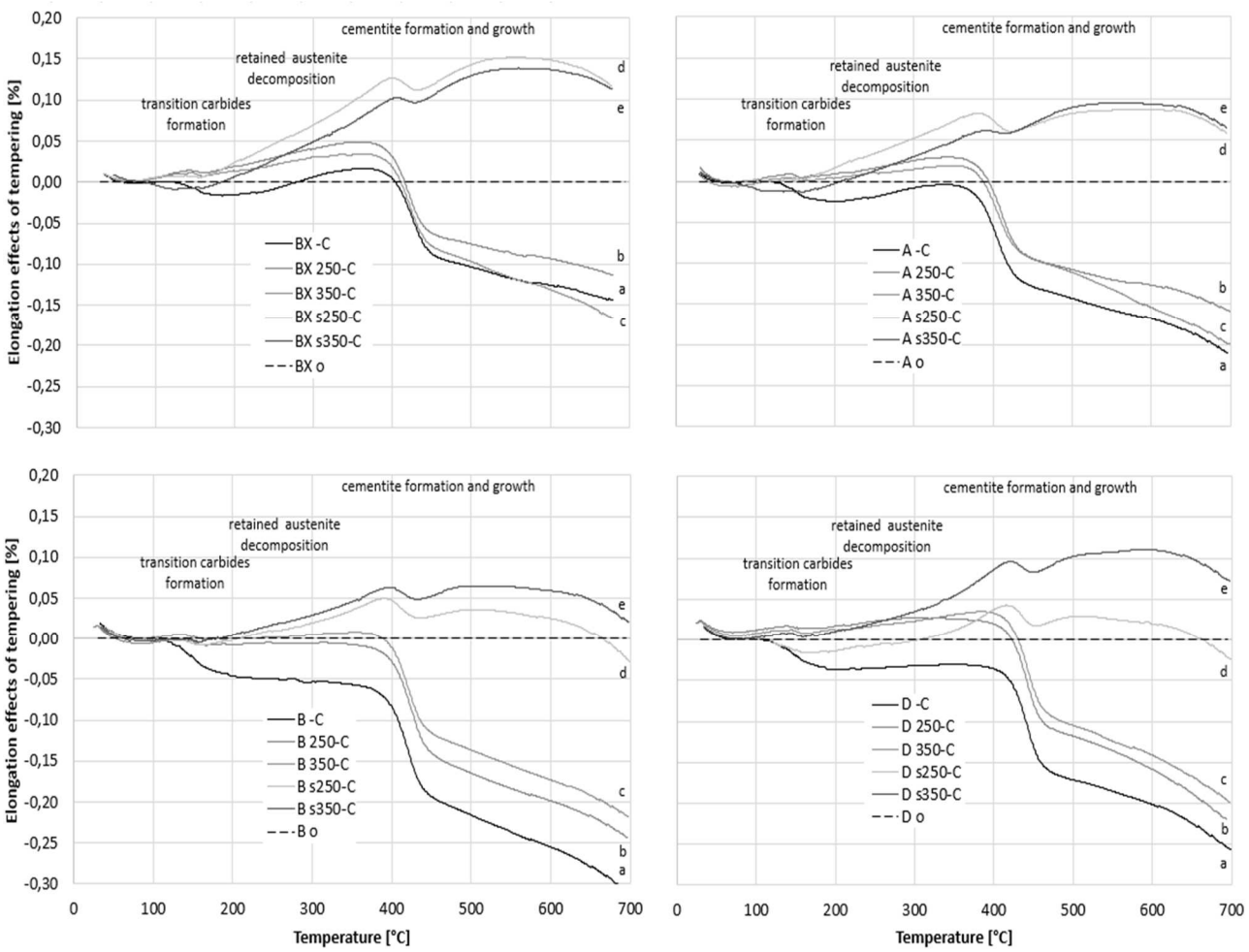

Fig. 1 *Dilatometry records of the anisothermal tempering process performed by continuous heating of samples after different preliminary processing; The curves are cleared of linear expansion upon heating, thus the black dashed line represents the baseline - simple heating course of material without any transformations; Any deviation from this baseline represents some kind of transformation event in the experimental material*

The dilatometry records by samples after quenching, the first tempering and 17% strain – yellow and red curves – are apparently different. The measurement of dilatation behavior during continuous heating of such samples shows only the hint of the negative deviation in the temperature range typical for the transition carbide formation. A very significant extension of experimental samples starts around the temperature of 150 °C. The growth of positive deviation from the linear course continues until to 550 °C, nevertheless in the temperature range close to 400 °C this growth is temporarily suspended by cementite precipitation and accompanying a decrease of the dilatometry curves. This effect related to cementite precipitation seems to be apparently weaker compared to dilatometry courses of samples without preliminary deformation. After reaching the temperature of 550 °C the dilatometry curves reveal the change of the course and their decrease is visible in the temperature range from 600 to 700 °C.

The influence of chemical composition on the dilatometry records shows some temperature shift by any transformation effects. The increasing Si content shifts the reactions to a longer time. Nevertheless, the shift is not very significant. This phenomenon is clearly visible if modification A (the lowest Si content) is directly compared to modification D (the highest Si content).

The difference between the behavior of deformed and non-deformed samples seems to be similar and very significant in all four steel modifications investigated. By the samples of modifications B and D, the positive deviation noticed during continuous heating of deformed samples compared to modifications A and BX is found to be lower. The course of dilatometry curves on samples without strain is very similar in all modifications. Nevertheless, the precipitation of carbides by the samples without strain seems to have a stronger effect on the materials containing higher Cu.

The results of isothermal heating in the dilatometer are presented in Fig. 2. Only materials B and BX were selected to evaluate isothermal tempering behavior.

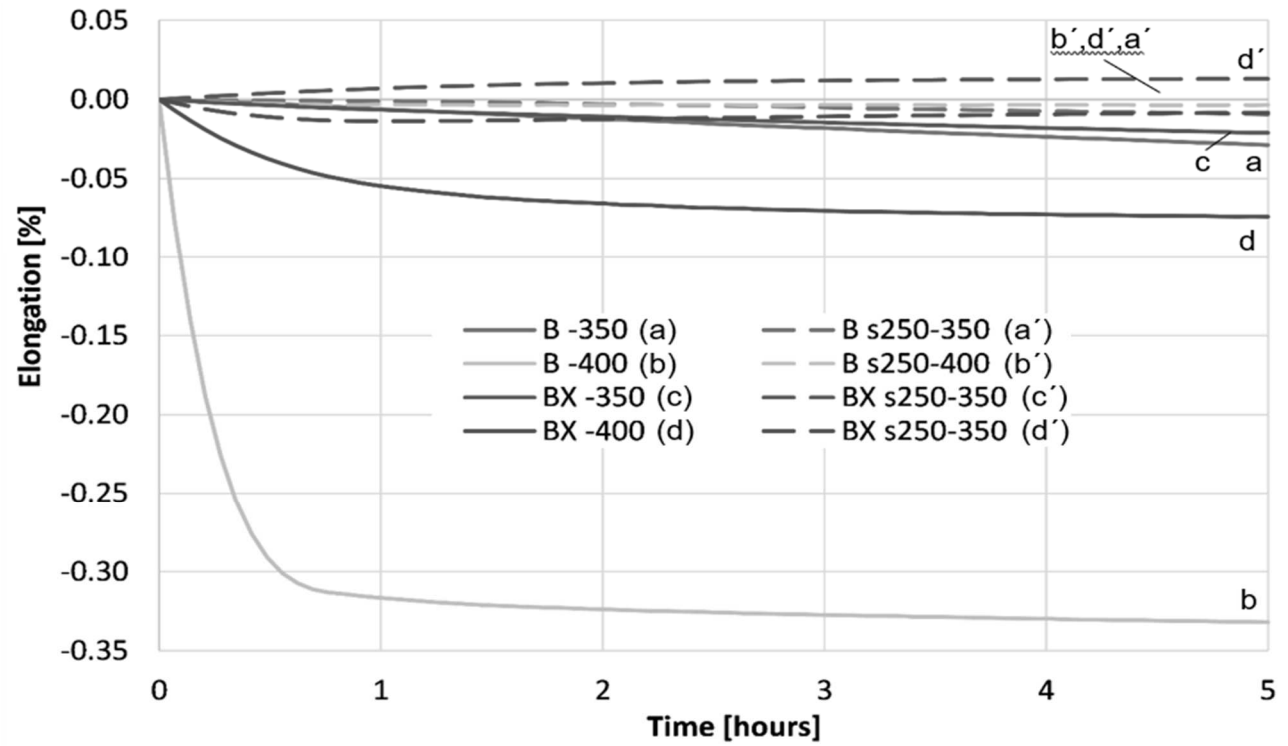

Fig. 2 *Dilatometry measurement of isothermal tempering after different preliminary processing*

The results of the isothermal measurement confirm the data obtained from the anisothermal measurement. The samples which were exposed to isothermal treatment just after quenching showed a decrease in their length related to transition carbides formation or cementite formation respectively during the heating in the dilatometer. On the contrary, the samples which were exposed to the first tempering and to the 17% strain after quenching show an increase in their length at both 350 and 400 °C tempering temperatures during the heating in the dilatometer. The contrast in the tempering effect is mainly visible evaluating the tempering temperature of 400 °C. Sample B -400 (b-curve: QT processing) shows a very significant shortening while sample B s250-400 (b´-curve: SAT processing) shows almost a zero change of the length. The deformation applied in a fundamental way restricts the precipitation of carbides. A similar trend is visible in all other samples subjected to comparison. A lower tempering temperature – 350 °C - shows a lower difference between QT and SAT samples indeed.

Also, the comparison of BX and B materials represents quite considerable differences visible mainly by 400 °C isothermal tempering. In this case, the precipitation in material B (sample B -400) records a much higher dilatation effect compared to material BX (sample BX -400). Both materials differ in Cu content, material B contains 1,48 % Cu while BX 0,12 % Cu only.

3.2 Metallography of samples after dilatometry exposition and hardness measurement

The microscopy of BX experimental material after isothermal low-temperature tempering was carried out with a focus on the comparison of samples with and without the strain before final tempering. The attention was paid mainly to the samples with the final tempering temperature of 350 °C. Nevertheless, the comparison with the tempering at 400 °C was done using SEM-SE (secondary electrons mode) technique.

The sample BX -350 (Fig. 3) microstructure shows the microstructure after quenching and tempering with a large number of transition carbides and a noticeable amount of retained austenite.

The sample BX s250-350 (Fig. 4) reveals the influence of the strain applied between double tempering. There are apparently fewer transition carbides and plenty of islands with a non-etched microstructure.

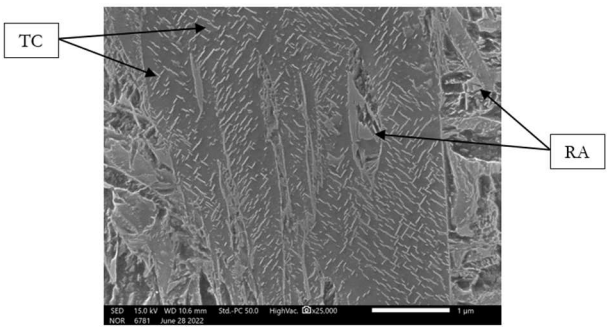

Fig. 3 *Microstructure of BX -350 (QT processed), TC – transition carbides, RA – retained austenite*

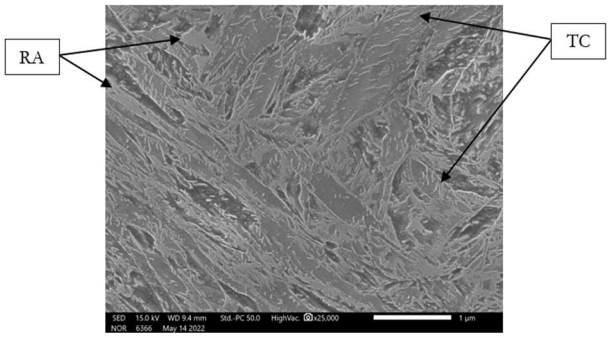

Fig. 4 *Microstructure of BX s250-350 (SAT processed), TC – transition carbides, RA – retained austenite*

Transition carbides start to be dissolved in both samples after tempering at 400 °C. Small cementite particles appear mainly on martensite lath boundaries and preliminary austenite grain boundaries. The occurrence of cementite is visible mainly in the microstructure of the BX -400 sample (Fig. 5), while plenty of non-etched islands are visible and cementite presence is not so apparent in the microstructure of the sample after SAT processing, see Fig. 6.

ECCI microscopic technique makes it possible to reveal some types of martensite substructures like twins respectively nano-twins. Fig. 7 shows the martensite lath with transition carbides which is grown by the twins' system across the boundary of the lath. These so-called long twins have typically no clear bonding, cross the boundary, and sometimes can have a great length.

The microstructure of SAT-processed samples includes nano-twins as well. In this case, the occurrence of so-called short twins is typical, see Fig. 8. Short twins are bounded inside one martensite lath and do not cross the boundary. In many cases, they fill the entire volume of the martensite lath. It is not possible to quantify the twin's occurrence in the samples after different processing from currently available data. The visibility of twins in the microstructure using the ECCI technique seems to be extremely sensitive to the angle between an electron beam and a twinning plane.

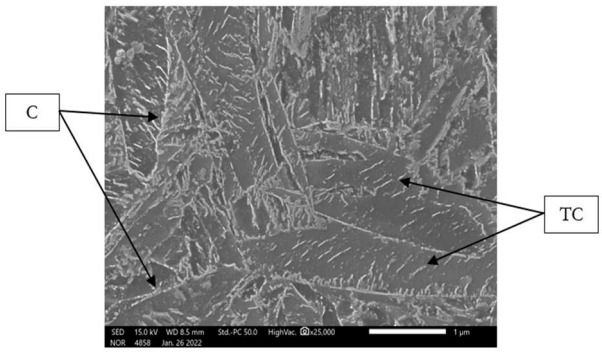

Fig. 5 *Microstructure of BX -400 (QT processed), TC – transition carbides, C – cementite*

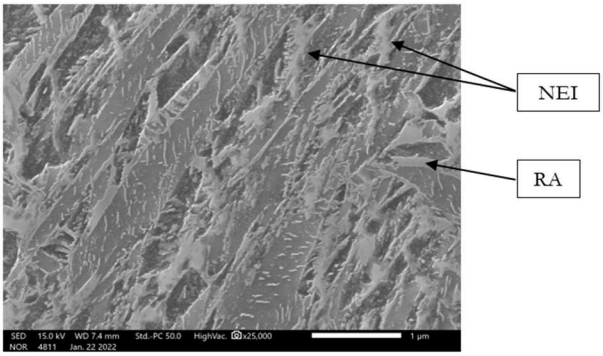

Fig. 6 *Microstructure of BX s250-400 (SAT processed), RA – retained austenite, NEI – non-etched island*

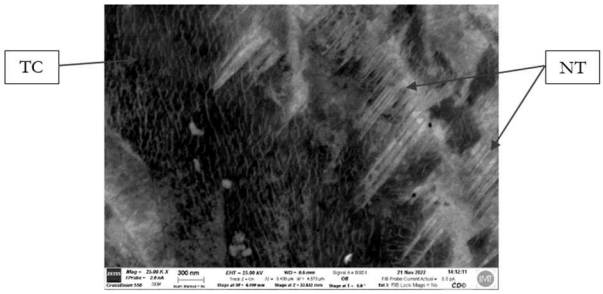

Fig. 7 *Microstructure of BX -350 (QT processed) using electron channeling contrast imaging (ECCI), TC – transition carbides, NT – nano-twins*

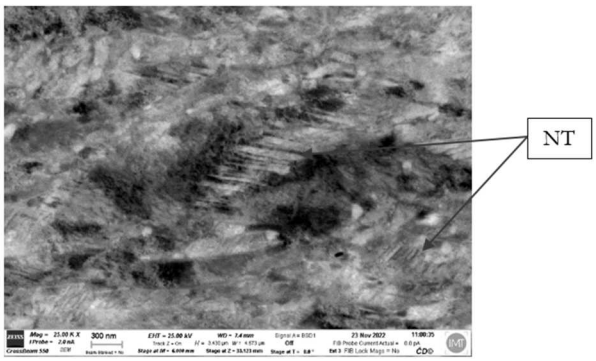

Fig. 8 *Microstructure of BX s250-350 (SAT processed) using electron channeling contrast imaging (ECCI), NT – nano-twins*

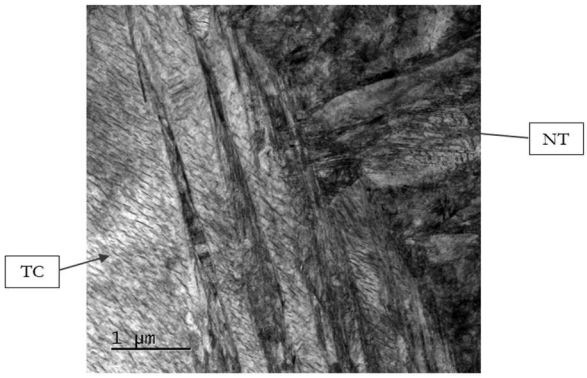

Fig. 9 *Microstructure of BX -350 (QT processed) using transmission electron microscopy, TC – transition carbides, NT – nano-twins*

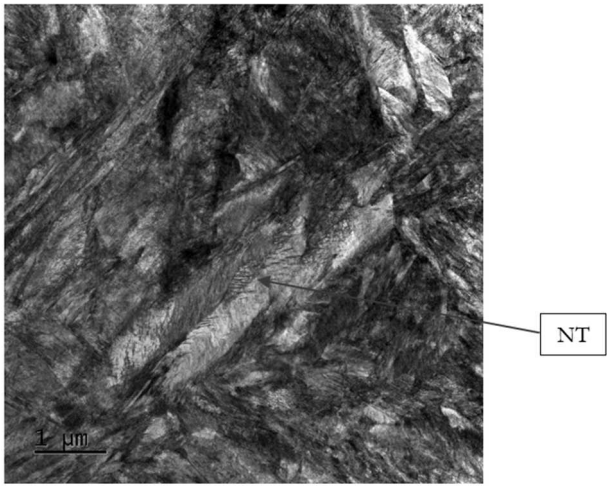

Fig. 10 *Microstructure of BX -350 (QT processed) using transmission electron microscopy, NT – nano-twins*

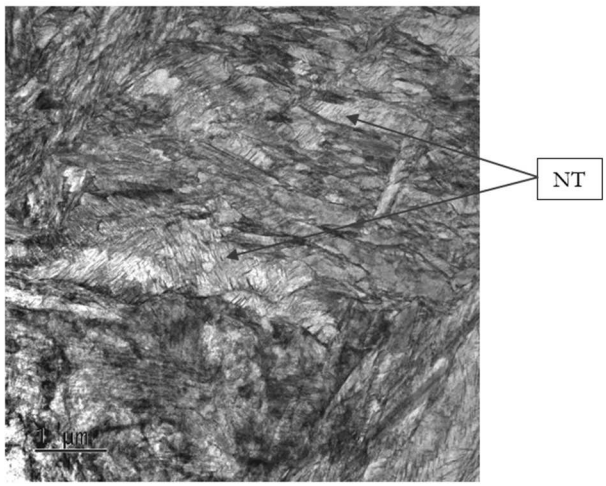

Fig. 11 *Microstructure of BX s250-350 (SAT processed) using transmission electron microscopy, NT – nano-twins*

Transmission electron microscopy also confirms the presence of twinned areas in the martensite. The pictures Fig. 9 and Fig. 10 show the co-existence of transition carbides and long twins in the same lath again. Larger martensite laths with higher amounts of transition carbides are visible in the QT-processed samples. The microstructure of the SAT-processed samples (Fig. 11 and Fig. 12) is apparently different, it has smaller substructure units in the martensite laths and usually short twins are detectable inside martensite laths. Those short twins are sometimes bonded by the martensite lath boundary, sometimes even by the substructure units boundary. Transition carbides are not detectable so often in this case. Small substructure units with crystallographic orientation related to the surrounding martensite laths are typical for SAT-processed samples. The substructure formation can be observed by QT-processed samples as well. Nevertheless, their size can usually be estimated to be larger compared to the microstructure after SAT processing.

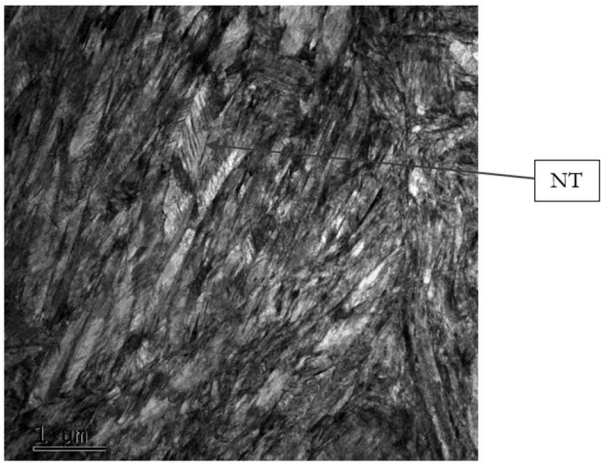

Fig. 12 *Microstructure of BX s250-350 (SAT processed) using transmission electron microscopy, NT – nano-twins*

The results of Vickers hardness measurement are stated in Tab. 4. Only materials B and BX were selected to evaluate hardness after QT and SAT processing.

Tab. 4 *Hardness of investigated samples*

Sample	B -350	B -400	BX -350	BX -400	B s250-350	B s250-400	BX s250-350	BX s250-400
HV 10	635	555	627	556	654	600	682	643
HRC converter	57,0	52,5	57,0	53,0	58,0	55,0	59,0	57,5

A significant increase in hardness can be observed after the strain and second tempering applications. SAT-exposed samples are 20 – 40 HV higher compared to QT samples with the same final tempering temperature. As to the chemical composition influence the presence of Cu did not affect the final hardness considerably, B and BX hardness results are very close together.

3.3 Discussion

The presented research studies the behavior of four spring steel 54SiCr6 modified by Cu and Si content during tempering using dilatometry and metallography analyses. The experimental material was processed after quenching by simple or double tempering or double tempering with inserted strain.

The last temperature exposure was performed in the dilatometer every time. The main output of this study is the evaluation of the influence of the inserted strain (performed between double tempering operations) on resulting and thermo-physical behavior, microstructure, and hardness of examined materials. A direct comparison of hardness, thermo-physical curves, and microstructure of QT-processed samples and SAT-processed samples was made.

The crucial influence of SAT processing shows both the hardness measurement and dilatometry analysis. The comparison of hardness values by samples after both QT and SAT processing with the same final tempering temperature show higher hardness by 20 - 40 HV after SAT processing by all materials tested.

The dilatometry temperature exposition simulates the tempering process by the steel, which is performed in different initial states. It is possible to observe the deviations of curves from the baseline by studying the dilatometry during continuous. These deviations represent any phase transformations. Dilatometry records of the samples after simple quenching without applied strain reveal mostly the negative deviation from the baseline in the whole temperature range (150 – 700 °C). Very intensive growth of this negative deviation is visible in the temperature range around 400 °C. On the contrary dilatometry records of samples after applied strain show the positive deviation from the baseline in the whole temperature range from 150 to 700 °C, the maximum of that deviation being between 500 - 600 °C. The curves representing the heating of samples after tempering without deformation reveal at first in the range from 150 to 300 °C the positive deviation, nevertheless around 400 °C the intensive decrease can be followed. The positive deviation turns into a negative one and then remains negative up to 700 °C.

To explain the above-described courses of dilatometry curves let us start to evaluate samples, which were continuously heated in a dilatometer just after quenching. This precipitation of transition carbides causes the first negative deviation from the baseline between 150 - 250 °C. It is a phenomenon visible by all black curves of all experimental materials. The change in the direction of the curve trajectory toward the baseline follows between 200 – 400 °C. This change could be caused by austenite decomposition. Secondly, a more important decrease in the negative deviation follows above 400 °C. This is the formation of cementite particles accompanied by considerable sample shortening. This phenomenon is probably running with variable intensity up to 700 °C. The curves representing the second tempering without the application of the strain (b,c-curves) have a similar course. In this case, the dilatometry almost does not detect low-temperature transition carbides precipitation because they precipitated during the first tempering at 250 or 350 °C respectively. These curves start with a positive deviation up to 350 °C and this course is followed by a strong decrease due to cementite formation again. Similarly like the samples after quenching also these samples have a negative deviation from the baseline in the whole temperature range between 400 and 700 °C, which is the effect of cementite formation again.

The course of dilatometer curves representing the behavior of samples after the first tempering and subsequent strain is significantly different almost in the whole investigated temperature range. The effect of transition carbides is very small and it remarkably starts at lower temperatures even by 120 °C. Above 130 °C the dilatometry curves achieve an increasing trend and positive deviation grows. It is not probably possible to explain this intensive elongation simply by retained austenite decomposition, another phenomenon could take place at the same time. Recovery processes during tempering after plastic strain, carbon diffusion into twins or into other crystal defects, and resulting carbide dissolution can be the related plots, causing an increase in the specific volume. Such phenomena together with the austenite decomposition reaction could justify the intensive positive deviation from the linear growth [19, 21, 22]. The cementite formation is detectable around the temperature of 400 °C, nevertheless considerably a smaller amount compared to the tempering without preliminary strain.

The dilatometry curve and the deviation from the baseline significantly grow between 450 and 550 °C, where recovery processes and carbides dissolution are probably more significant than precipitation of new carbides. By the temperatures above 550 °C the deviation decreases towards the baseline. In this case, the cementite precipitation seems to be more dominant compared to carbide dissolution.

The isothermal dilatometry measurement was found to be in accordance with the above-presented results and hypothesis. A dilatometry simulation of isothermal tempering at 350 and 400 °C respectively performed without the preliminary strain reveals the decrease in the sample length due to carbides precipitation in both cases. Transition carbides precipitation prevails at the temperature of 350 °C (a moderate length decrease) and cementite precipitation is dominant at 400 °C (a more significant decline).

Metallography analyses are also in accordance with the stated assumptions. Scanning electron microscopy shows clearly more transition carbides in the microstructure after simple tempering in the range from 250 to 400 °C compared to the samples tempered after the preliminary strain. There is a loss of carbides during the tempering performed after strain. Transmission microscopy and ECCI analysis

made plenty of twins in the microstructure visible. Observing these structure defects, their origin of creation is not clear. Some of them exist in the material from the quenching operation nevertheless, there is also the hypothesis that some of them arose during the strain application or even after that. The formation of twins during quenching or just after quenching in hardened steels has been described by many authors [23-25]. The formation of twins in martensite after the deformation or even during the following tempering is difficult to find in the literature.

Important knowledge gained from a microscopic observation is the difference between the martensitic lath substructure after QT and SAT processing. Martensitic laths are segmented into smaller subgrains, this finding is in accordance with the literature sources, where substructures of bcc martensite are often encountered [26-28]. This segmentation seems to be considerably more pronounced after SAT processing – see Fig. 7 to Fig. 12. Furthermore, some segments are filled by transformation twins. The used experimental methods do not allow quantifying twins in the martensitic matrix. Therefore, it is not possible to compare the number of twins before the strain and after that. Thus, it was not possible to evaluate if the samples after SAT processing contain more or less twins compared to the samples after QT processing. The intensive refinement of the substructure and the effect of twins can be the reasons for the significant increase in hardness and other mechanical properties.

4 Conclusion

The main goal of the presented study was the comparison of spring steel behavior during standard one-step tempering after quenching and during SAT processing. Both continuous heating and isothermal dilatometry showed considerable differences. Intensive transition carbides precipitation and cementite formation up to 700 °C can follow during simple one-step tempering. The precipitation processes were largely suppressed after the strain application. The lower content of carbides in the samples after SAT processing was detected also by metallography analysis using the scanning and transmission electron microscopy. Besides the lower precipitation level, even some degree of dissolution of carbides during tempering could be the explanation for dilatometry records. This way, more carbon content remained in the solid solution after SAT processing. Similar thermo-physical behavior revealed in all steel modifications. Only a relatively small deviation could be followed. Nevertheless, their behavior was basically the same or very similar.

SAT process introduced significantly higher hardness into the material compared to the QT process. Deformation strengthening in the synergy with martensitic transformation and precipitation strengthening shifted the hardness considerably higher. A finer martensite substructure after SAT with common nano-twins could be the reason for significant strengthening after SAT processing.

The intensity of transition carbides precipitation was apparently influenced by Cu content. All samples containing 1,5 % Cu revealed more intensive precipitation of transition carbides compared to conventional steel 54SiCr6 (BX) with minor Cu content. This phenomenon was observed during both continuous heating dilatometry and isothermal dilatometry. Growing Si content caused a shift of the cementite formation to a longer time.

Acknowledgement

This paper was created within the project National Centre of Competence ENGINEERING, No. TN02000018, which is co-financed from the state budget by the Technology agency of the Czech Republic under the National Centres of Competence Programme and by the European Union – NextGenerationEU within the National Recovery Plan.

References

[1] CHEN, K., JIANG, Z., LIU, F., YU, J., LI, Y., GONG, W. and CHEN, C. (2019). Effect of quenching and tempering temperature on microstructure and tensile properties of microalloyed ultra-high strength suspension spring steel. In: *Materials Science and Engineering A*, Vol. 766, pp. 1-11, ISSN 09215093.

[2] HUANG, S., LI, L., PENG, Z., XING, X., GAO, J. and WANG, B. (2021). Effect of tempering time on microstructure and properties of 65Si2CrV spring steel. In: *Journal of Physics: Conference Series*, Vol. 2044, No. 1, pp. 1–7, ISSN 17426596.

[3] MATJEKE, V.J., MUKWEVHO, G., MALEKA, A.M. and VAN DER MERWE, J.W. (2018). Effect of heat treatment on strength and ductility of 52CrMoV4 spring steel. In: *IOP Conference Series: Materials Science and Engineering*, Vol. 430, No. 1, pp. 1-7, ISSN 1757899X.

[4] JENÍČEK, Š., OPATOVÁ, K., HAJŠMAN, J., VOREL, I. (2022). Evolution of Mechanical Properties and Microstructure in Q&P Processed Unconventional Medium-Carbon Silicon Steel and Comparison between Q&P Processing, Quenching and Tempering, and Austemperingfor. In: *Manufacturing Technology*, Vol. 22, No. 2, pp. 146-155, ISSN 12132489.

[5] HUNKEL, M., DONG, J., EPP, J., KAISER, D., DIETRICH, S., SCHULZE, V., RAJAEI, A., HALLSTEDT, B. and BROECKMANN, C. (2020). Comparative study of the tempering behavior of different martensitic steels by means of in-situ diffractometry and dilatometry. In: *Materials*, Vol. 13, No. 22, pp. 1–15, ISSN 19961944.

[6] JUNG, M., LEE, S.J. and LEE, Y.K. (2009). Microstructural and dilatational changes during tempering and tempering kinetics in martensitic medium-carbon steel. In: *Metallurgical and Materials Transactions A: Physical Metallurgy and Materials Science*, Vol. 40, No. 3, pp. 551–559, ISSN 10735623.

[7] JENÍČEK, Š., VRTÁČEK, J., VOREL, I., JANDA, T. (2020). Dilatometric Identification of Bainitic Transformation during Q-P Processing of 42SiCr Medium Carbon Steel. In: *Manufacturing Technology*, Vol. 20, No. 3, pp. 327-334, ISSN 12132489.

[8] BARRERA-VILLATORO, E.F., VÁZQUEZ-GÓMEZ, O., GALLEGOS-PÉREZ, A.I., VERGARA-HERNÁNDEZ, H.J., LÓPEZ-MARTÍNEZ, E. and GARNICA-GONZÁLEZ, P. (2021). Dilatometric Analysis of Tempering Kinetics in a Cr–Mo–V Medium-Carbon Steel. In: *Minerals, Metals and Materials Series*, Vol. 5, pp. 902–908, ISSN 23671696.

[9] SALVETR, P., GOKHMAN, A., NOVÝ, Z., MOTYČKA, P. and KOTOUS, J. (2021). Effect of 1.5 wt% copper addition and various contents of silicon on mechanical properties of 1.7102 medium carbon steel. In: *Materials*, Vol. 14, No. 18, pp. 1-19, ISSN 19961944.

[10] KUČEROVÁ, L., BYSTRIANSKÝ, M., JENÍČEK, Š. (2017) The Effect of Annealing Temperature on Microstructure and Mechanical Properties of Lightweight Steel with Increased Aluminium Content. In: Manufacturing Technology, Vol. 17, No. 6, pp. 881-887, ISSN 12132489.

[11] ZHANG, W. and XU, J. (2022). Advanced lightweight materials for Automobiles: A review. In: *Materials & Design*, Vol. 221, No. 110994, pp. 1–20, ISSN 0264-1275.

[12] KOTOUS, J., SALVETR, P. and PROCHÁZKA, R. (2021). New approach to heat treatment of spring steel. In: *IOP Conference Series: Materials Science and Engineering*, Vol. 1178, No. 1, pp. 1-6, ISSN 1757-8981.

[13] HU, W., LI, J., LI, K., ZHANG, T. and REN, X. (2021). Improving the cycle fatigue life of spring steel by a novel thermal cycling process. In: *Materials Research Express*, Vol. 8, No. 5, pp. 1–5, ISSN 20531591.

[14] GUBELJAK, N., CHAPETTI, M.D., PREDAN, J. and SENČIČ, B. (2011). Variation of fatigue threshold of spring steel with prestressing. In: *Procedia Engineering*, Vol. 10, pp. 3339–3344, ISSN 18777058.

[15] ZHANG, J.M., LI, S.X., YANG, Z.G., LI, G.Y., HUI, W.J. and WENG, Y.Q. (2007). Influence of inclusion size on fatigue behavior of high strength steels in the gigacycle fatigue regime. In: *International Journal of Fatigue*, Vol. 29, No. 4, pp. 765–771, ISSN 01421123.

[16] LIU, Y.B., LI, Y.D., LI, S.X., YANG, Z.G., CHEN, S.M., HUI, W.J. and WENG, Y.Q. (2010). Prediction of the S-N curves of high-strength steels in the very high cycle fatigue regime. In: *International Journal of Fatigue*, Vol. 32, No. 8, pp. 1351–1357, ISSN 01421123.

[17] BARANI, A.A. and PONGE, D. (2007). Optimized Thermomechanical Treatment for Strong and Ductile Martensitic Steels. In: *Materials Science Forum*, Vol. 539-543, pp. 4526-4531.

[18] ARDEHALI BARANI, A., PONGE, D. and RAABE, D. (2006). Refinement of grain boundary carbides in a Si-Cr spring steel by thermomechanical treatment. In: *Materials Science and Engineering A*, Vol. 426, No. 1–2, pp. 194–201, ISSN 09215093.

[19] NOVÝ, Z., SALVETR, P., KOTOUS, J., MOTYČKA, P., GOKHMAN, A., DONIK, Č. and DŽUGAN, J. (2022). Enhanced Spring Steel's Strength Using Strain Assisted Tempering. In: *Materials*, Vol. 15, No. 20, pp. 1–20, ISSN 19961944.

[20] PROCHÁZKA, R., STEHLÍK, A., KOTOUS, J., SALVETR, P., BUCKI, T., STRÁNSKÝ, O. and ZULIC, S. (2023). Fatigue Properties of Spring Steels after Advanced Processing. In: *Materials*, Vol. 16, No. 3327, pp. 1–13.

[21] GALINDO-NAVA, E.I. and RIVERA-DÍAZ-DEL-CASTILLO, P.E.J. (2016). Understanding the factors controlling the hardness in martensitic steels. In: *Scripta Materialia*, Vol. 110, pp. 96–100, ISSN 13596462.

[22] KRAUSS, G. (2017). Tempering of Lath Martensite in Low and Medium Carbon Steels: Assessment and Challenges. In: *Steel Research International*, Vol. 88, No. 10, pp. 1–18, ISSN 1869344X.

[23] ZHANG, P., CHEN, Y., XIAO, W., PING, D. and ZHAO, X. (2016). Twin structure of the lath martensite in low carbon steel. In: *Progress in Natural Science: Materials International*, Vol. 26, No. 2, pp. 169–172, ISSN 17455391.

[24] LIU, T., LIANG, L., RAABE, D. and DAI, L. (2023). The martensitic transition pathway in steel. In: *Journal of Materials Science and Technology*, Vol. 134, pp. 244–253, ISSN 10050302.

[25] KELLY, P.M. and NUTTING, J. (1960). The martensite transformation in carbon steels. In: *Proceedings of the Royal Society of London. Series A. Mathematical and Physical Sciences*, Vol. 259, No. 1296, pp. 45–58, ISSN 0080-4630.

[26] SUN, J.J., LIU, Y.N., ZHU, Y.T., LIAN, F.L., LIU, H.J., JIANG, T., GUO, S.W., LIU, W.Q. and REN, X.B. (2017). Super-strong dislocation-structured high-carbon martensite steel. In: *Scientific Reports*, Vol. 7, No. 1, pp. 1–7, ISSN 20452322.

[27] MAKI, T. (2012). Phase Transformations in Steels: Morphology and substructure of martensite in steels. In: *Woodhead Publishing Series in Metals and Surface Engineering*, Vol. 2, pp. 34-58.

[28] JI, Y., LIU, Z. and REN, H. (2012). Stacking fault substructure of martensite in steel. In: *Applied Mechanics and Materials*, Vol. 121–126, pp. 3493–3497, ISSN 16609336.